Geophysical Research Letters

RESEARCH LETTER
10.1029/2018GL080226

Key Points:
- At the equator, zonal velocity oscillations of the 17-day TIW are identified, in complement to the well-known meridional oscillations
- The resulting NE-SW oscillating, equatorial mode TIW differs from both the Yanai wave at the equator or the TIV north of the equator
- The westward anomalous velocities induce the strongest vertical shear in the subsurface ocean, favoring the equatorial turbulent mixing

Correspondence to:
C. Liu and X. Wang,
chuanyu.liu@qdio.ac.cn;
wangxiaowei@qdio.ac.cn

Citation:
Liu, C., Wang, X., Köhl, A., Wang, F., & Liu, Z. (2019). The northeast-southwest oscillating equatorial mode of the tropical instability wave and its impact on equatorial mixing. *Geophysical Research Letters*, *46*, 218–225. https://doi.org/10.1029/2018GL080226

Received 29 AUG 2018
Accepted 4 DEC 2018
Accepted article online 10 DEC 2018
Published online 3 JAN 2019

The Northeast-Southwest Oscillating Equatorial Mode of the Tropical Instability Wave and Its Impact on Equatorial Mixing

Chuanyu Liu[1,2,3,4], Xiaowei Wang[1,2,3,4], Armin Köhl[5], Fan Wang[1,2,3,4], and Zhiyu Liu[6]

[1]CAS Key Laboratory of Ocean Circulation and Waves, Institute of Oceanology, Chinese Academy of Sciences, Qingdao, China, [2]Marine Dynamic Process and Climate Function Laboratory, Pilot National Laboratory for Marine Science and Technology (Qingdao) (QNLM), Qingdao, China, [3]University of the Chinese Academy of Sciences, Beijing, China, [4]Center for Ocean Mega-Science, Chinese Academy of Sciences, Qingdao, China, [5]Institute of Oceanography, University of Hamburg, Hamburg, Germany, [6]State Key Laboratory of Marine Environmental Science, and Department of Physical Oceanography, College of Ocean and Earth Sciences, Xiamen University, Xiamen, China

Abstract The tropical instability waves (TIWs) in the eastern Pacific consist of waves with central periods of about 33 and 17 days. While the former manifest as vortices north of the equator, and are known to modulate diapycnal mixing at their southern edge, the latter remain largely unexplored. Here the structure of the 17-day TIWs and the mechanism through which they may influence equatorial mixing are investigated based on long term in situ measurements and reanalysis data. Different from the well-recognized meridional velocity oscillation, the 17-day TIWs are found to induce northeast-southwest (NE-SW) velocity oscillations. They are confined within but asymmetric about the equator, differing from free Yanai waves, which they were commonly assumed to resemble. The vertical shear associated with the westward anomalous velocity superimposes on the shear of the mean flow, resulting in the strongest shear in the upper thermocline that is expected to facilitate diapycnal mixing therein.

Plain Language Summary Observed from satellites, the tropical instability wave (TIW) in the eastern tropical Pacific Ocean is a 1,000-km-long gigantic combination of waves and vortexes. It emerges between the energetic zonally interleaving equatorial currents, impacts the atmosphere, and transfers enormous energy to the western Pacific Ocean and to the deep ocean as well—one of the research foci for both physical oceanographers and meteorologists. However, the structures of its huge body, and the associated complicated smaller-scale processes, remain unrevealed, primarily because the measurements that have been conducted, usually by research vessels, are too limited to derive a full picture. Here based on long-term observations at a hotspot of TIW and 4-D numerical model outputs, we identify the structure of TIW at the equator, which manifests as a pair of slanted clockwise and anticlockwise vortexes, and induces strong east-west oscillations. We also find the most efficient mechanism for the TIW to strengthen vertical velocity shear, shear instability, and ocean turbulent mixing. The findings therefore are important for understanding the TIW dynamics, TIWs' signatures in atmosphere-ocean interactions, and their impact on vertical heat transport from warmer sea surface to colder subsurface layers of the ocean.

1. Introduction

Tropical instability waves (TIWs) are important for meridional ocean heat transport in the eastern Pacific cold tongue region owing to their energetic meridional oscillations (e.g., Menkes et al., 2006). They not only result in coupled atmosphere-ocean interactions at TIW scales but also impact climate variability at larger scales (e.g., Pezzi et al., 2004; Zhang & Busalacchi, 2008). In addition, they play an important role in vertical heat transport from sea surface to the thermocline via promoting vertical mixing in the upper ocean (Inoue et al., 2012; Liu et al., 2016; Moum et al., 2009, 2013). The mixing-induced surface cooling is able to further influence the seasonal and El Niño–Southern Oscillation-related variations of the sea surface temperature (Moum et al., 2009, 2013). Specifically, it has been demonstrated that, at equator 140°W (hereafter Eq140W)—a hotpot of TIWs of the Pacific Ocean—the TIW-induced vertical shear accounts for more than 50% of the total shear in the upper ocean (Liu et al., 2016), and the meridional velocity oscillation brings 30% more decrement of the Richardson number (Moum et al., 2009), which can potentially enhance mixing therein. In particular, based on Lagrangian measurements, Lien et al. (2008) revealed that, along the equator,

mixing is enhanced in the warm phases of TIWs. Holmes and Thomas (2015) (hereafter HT15), using model results, demonstrated that the enhanced westward vertical shear at the leading edges of the TIW warm phases is primarily responsible for the enhanced mixing.

Lyman et al. (2007; hereafter L07) suggested two modes of TIWs in this region: One has a central period of ~33 days and the other ~17 days (referred to as 33-day TIW and 17-day TIW, respectively, hereafter). The 33-day TIW refers to the northern mode of TIW, which manifests as an anticyclonic vortex with warm edge along the equator and cold cusp to the north (Flament et al., 1996; Kennan & Flament, 2000). This vortex can be clearly identified within 2°–8°N of the eastern Pacific from satellite and in situ measurements and is known as the tropical instability vortex (TIV; see Holmes et al., 2014, for a review). In comparison, relatively less is known about the 17-day TIW. On the one hand, L07 demonstrated that it locates south of the TIV, and Flament et al. (1996) and Kennan and Flament (2000) suggested that it has larger propagation speed; however, the horizontal structure of the 17-day TIW, the regime where it emerges and how it may communicate with the 33-day TIW, to our knowledge, have not been revealed. On the other hand, both of the observational work like Moum et al. (2009) and Lien et al. (2008) and the modeling work like Menkes et al. (2006) and HT15, were focusing on the entire TIW flow field at/near the equator and have not clearly separated the effect of the 17-day TIW on equatorial mixing. Therefore, the aim of the present work is to identify the structure of the 17-day TIW and investigate the mechanism through which it may impact the equatorial mixing.

2. Data

Two ocean data sets were employed. One is the *hourly* ocean temperature, salinity, and velocity data at Eq140W obtained by the Tropical Atmosphere-Ocean (TAO) observations (McPhaden, 1995); the other is the 3-hourly outputs of the global 1/12° Hybrid Coordinate Ocean Model/Navy Coupled Ocean Data Assimilation (HYCOM/NCODA) reanalysis (Cummings & Smedstad, 2013). They are available at http://www.pmel.noaa.gov/tao/data_deliv and http://apdrc.soest.hawaii.edu/datadoc/hycom_global_reana.php, respectively. The time periods for analysis are described in the following section.

3. Results

3.1. Dominance of the 17-Day TIW at Eq140W and the Northeast-Southwestward (NE-SW) Velocity Oscillations

Here we demonstrate that, in addition to the well-recognized meridional oscillation, TIWs at Eq140W also oscillate zonally at the same frequencies and eventually have a preferred oscillation direction: NE-SW. Following L07, we chose the persistent La Niña years, from January 1998 to December 2000, when TIWs were strong, for analysis. We first isolated both meridional and zonal TIW velocities by 10- to 60-day band-pass filtering the hourly TAO velocities at each depth, and then identified the central frequencies/periods of the TIW variability using a power spectral density (PSD) analysis. The depth-frequency/period distribution of PSD of the band-passed meridional (v) velocity component (Figure 1b) shows a peak at ~17.5 days above the thermocline center (which is at ~100 m). The signals are the 17-day TIWs discussed by L07. Moreover, PSD of the band-passed zonal (u) velocity component (Figure 1a) also displays a peak at ~17.5 days above ~100 m, though a little broader banded (14–24 days) in the upper flank of the thermocline (50–100 m), and of smaller magnitude than the v component.

The 33-day TIWs (i.e., TIVs, periods within 25–40 days) are also shown in the figures but are less significant in the u component and have much smaller magnitude in the v component than their 17-day counterpart. This is true not only during the study period but also during the entire TAO durations (not shown). This suggests that the TIWs at the equator are dominated by the 17-day TIWs (which can also be inferred from the black and green curves in Figure 1d).

The consistency in oscillating periods between the two components of the 17-day TIW may indicate regularly coherent movement of the TIW at this location, which is further determined by coherence analysis (Halpern et al., 1988; Qiao & Weisberg, 1995). Figure 1c shows the coherence variances between the two components for the 3-year period. The values of coherence variance are all at 95% confidence level; however, only those >0.5 are considered significant (i.e., linearly related; Halpern et al., 1988). It shows that the two components are coherent at 15–19 days from 35 m to the lower flank of the thermocline; phase angles exist but vary within a small range: 0.2–0.4 radians (the u leads). Both components are also coherent at 20–24 days

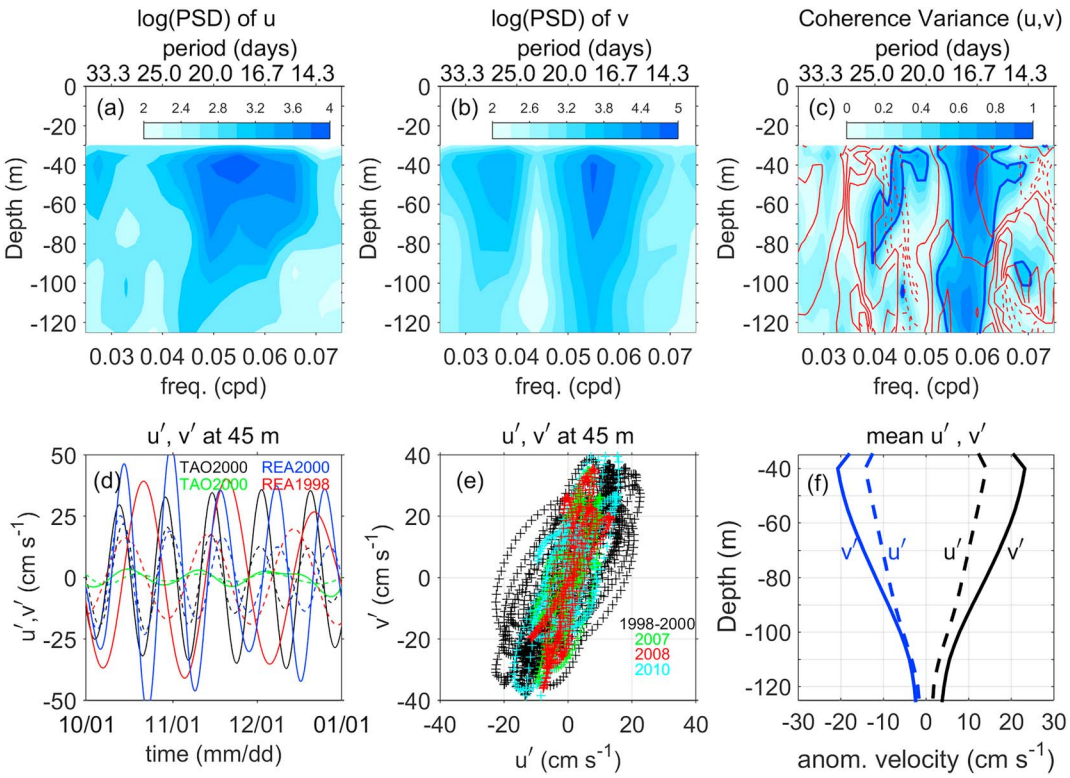

Figure 1. PSD of the 10- to 60-day band-passed (a) *u* and (b) *v* velocity components. (c) Coherence variance (shading; isoline of 0.5 is highlighted) and phase difference between the two components (red contours). Plots of (a)–(c) are based on the 3-year (1998–2000) TAO data, and the unit cpd is short for cycles per day. (d) Time series over October–December of the 17-day (black and blue) and 33-day (green and red) TIWs at 45 m; dashed (solid) curves are for the *u* (*v*) components. The symbol TAO2000 is for year 2000 of TAO data, and so as the others; all plots are for Eq140W except for the red curves, which are for 4°N, 140°W. (e) Hodograph of u' and v' of the 17-day tropical instability waves from TAO data (at 45 m); colors and insets denote year-by-year variations. (f) Mean u' and v' of the 17-day TIWs from TAO data, averaged at phases of maximum eastward (black) and westward (blue) anomalous velocities at 45 m; the degree of freedom is over 20. In (e) and (f), only data of TIW conditions (120-day low-passed, 30- to 70-m averaged TIW kinetic energy (TIWKE) $> 0.04\ m^2/s^2$; refer to Liu et al., 2016) is used. PSD = power spectral density; TAO = Tropical Atmosphere-Ocean; TIW = tropical instability wave.

above the thermocline. The coherency can be illustrated by the time series of 12–24 days band-passed velocities (representative for the 17-day TIW) of the two components (Figure 1d, black and blue) from both TAO and the reanalysis. In contrast, the 25- to 40-day band-passed (representative for the 33-day TIV) velocities do not show such coherence (green).

The results imply that the anomalous movements of the 17-day TIWs at Eq140W may display rectilinear or rotary oscillations (subject to the nonnegligible phase lags between the two components) oriented toward NE-SW, as shown by the hodograph of the 12- to 24-day band-passed velocities in Figure 1e. The hodograph shows an ellipse (periphery of the markers) with the semimajor axis-oriented NE-SW. The magnitude of the *u* component is over 20 cm/s, about a half of the *v* component (~40 cm/s) for the year 1998–2000. The NE-SW-oriented ellipses clearly demonstrate that the equatorial mode TIW oscillates primarily along northeast-southwest (NE-SW); we thereby call it NE-SW oscillation. In contrast, neither rotary oscillation nor preferred direction was found for the 33-day TIWs at the equator (not shown). The NE-SW oscillation is vertically coherent above the thermocline, though the magnitude decreases with depth; this is demonstrated by the mean anomalous TIW velocities (ATVs) that are averaged at phases of either maximum westward or maximum eastward ATVs at 45 m (Figure 1f).

The SW-NE orientation also shows interannual modulations. A significant feature is that it is most pronounced during La Niña condition. As an example, Figure 1e shows the oscillation at 45 m for other La Niña years 2007, 2008, and 2010 based also on TAO data at Eq140W. They vary in both magnitudes and tilt slopes, but the direction is kept roughly at NE-SW. In contrast, no orientation preference can be clearly identified during most El Niño or neutral conditions. This may explain why the 1990–1991 (neutral conditions) observations

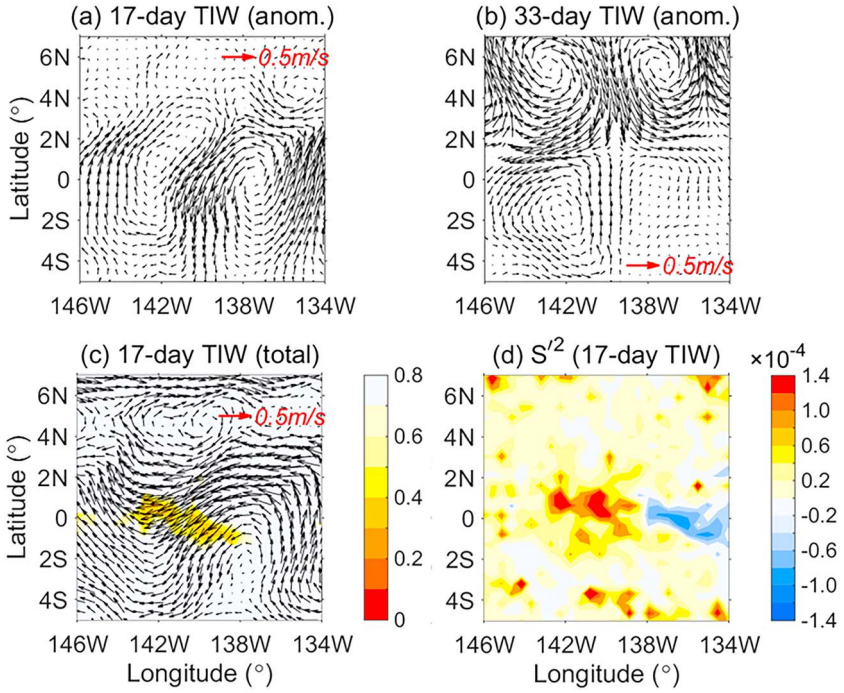

Figure 2. Mean ATVs at 45 m of the (a) 17-day TIW and (b) the 33-day TIW. (c) Mean total current (vector) and mean *Ri* (shading) and (d) mean shear squared increment of $S_u^{'2} + S_v^{'2}$ (s^{-2}) of the 17-day TIW. The mean *Ri* in (c) is calculated as $\overline{Ri} = \overline{N^2}/\overline{S^2}$, where $\overline{(\,)}$ denotes time average over the mentioned period; the total current is the sum of ATV and 40-day low-passed flow. Values in (a), (c), and (d) are averaged at phases of maximum southward ATVs at 45 m of the Eq140W for October–December 2000, while values in (b) are averaged at phases of maximum *southward* ATVs at 45 m of 4°N, 140°W for October–December 1998 (time series displayed in Figure 1d). Both S^2 and N^2 are calculated between model levels 45 and 50 m with forward difference. ATV = anomalous TIW velocity; TIW = tropical instability wave.

(Qiao & Weisberg, 1995) have shown an NE-SW-oriented ellipse, albeit with a large ratio between the *v* and *u* components. The interannual variation is presumably due to the variation of the background conditions that generate and maintain TIWs (Johnson & Proehl, 2004; Pezzi et al., 2006; Proehl, 1998; Yu et al., 1995).

3.2. The Horizontal Structure of the 17-Day TIW

Using high-resolution HYCOM/NCODA reanalysis data, we constructed the mean characteristics of both the 17-day TIWs and 33-day TIVs (Figure 2), which show distinguishingly different structures as anticipated. Figures 2a and 2c, respectively, show the mean ATVs and the corresponding total currents of the 17-day TIWs in October–December 2000 (refer Figure 1d for time series). During the period, this TIW mode had a mean westward phase speed of 0.74 m/s (estimated at Eq140W). The anomalous pattern (Figure 2a) manifested as a pair of equatorially trapped, clockwise and anticlockwise vortexes; in particular, the vortexes were visibly squashed and tilted toward NE-SW, resulting in an asymmetry about the equator. The vortexes are associated with NE-SW velocity oscillations, consistent with the TAO measurements. In addition, the coherency seems more evident in the eastern than in the western portion. L07 argued, without showing horizontal structures, that the 17-day TIW resembles the Yanai wave, which was then supported by dispersion relation analysis (Shinoda, 2010). However, the NE-SW tilt and asymmetry here make the 17-day TIW different from a free Yanai wave, which manifests as regular clockwise and anticlockwise vortexes, antisymmetric about the equator, and with no zonal component of velocity at the equator. Instead, the positive definite covariance of the NE-SW oscillating ATVs, $\overline{u'v'}$, that is, the Reynolds stress, an agent of energy transfer via barotropic instability between the instability wave and the horizontally sheared mean flow (Masina et al., 1999), implies that such pattern is reflecting the instability nature (barotropic instability) of the TIWs. (Another energy source for TIWs is baroclinic instability, and the relative contributions of both instabilities can be modulated by lateral mixing [Pezzi & Richards, 2003]). The sign of $\overline{u'v'}$ due to the 17-day TIW, as well as that due to the

33-day TIW as shown below, is the same as in Johnson and Proehl (2004). We note that, TIWs of similar horizontal characteristics (i.e., clockwise and anticlockwise vortexes) have been found in theoretical studies, but they are either antisymmetric about the equator (McCreary & Yu, 1992) or northward shifted from the equator (Yu et al., 1995) due to symmetric or asymmetric equatorial ocean states. Neither theoretical work nor direct measurements, to our knowledge, have revealed the pair of tilted TIW vortexes.

The corresponding total current (Figure 2c) manifests as a flat "S-shaped" wave, rather than a closed vortex due to the westward South Equatorial Current. The wave is confined within the equatorial band (±4° in latitude), with a wave length about 10°, similar to previous estimates. At the center of the wave, the magnitude of the velocity is about 0.5 m/s.

For comparison, Figures 2b shows the ATVs of the 33-day TIWs in October–December 1998. During the period, this TIW had a mean westward phase speed of 0.40 m/s (estimated at 4°N), smaller than the 17-day TIW (0.74 m/s). This indicates that the two TIW modes cannot be phase locked or move coherently. The anomalous TIW manifested as two pairs of clockwise and anticlockwise vortexes in the Northern (centered at 5°N) and Southern (centered at 2°S) Hemispheres, respectively. The corresponding total current manifested as an anticyclonic TIV around 144°W, 5°N with a radius of about 4° (not shown), consistent with previous observations (Flament et al., 1996; Kennan & Flament, 2000) and model simulations (e.g., Menkes et al., 2006). This pattern, as argued by L07, likely resembles the first meridional mode of the first baroclinic Rossby wave; however, differences are also apparent from a free Rossby wave. First, the four vortexes are not symmetric about the equator but about the latitude of ~1°N. Second, the northern portion displays southeast-northwest, rather than north-south, oscillating velocities, yielding negative $\overline{u'v'}$, which may also imply maintenance of the wave (partly) by barotropic instability. It can be expected that the oscillation may be interannually modulated or modulated by other equatorial processes, such as Kelvin waves (Holmes & Thomas, 2016). Note that the TIWs are also associated with zonal velocity oscillations along the equator. Finally, the northern portion is much stronger than the southern portion (particularly, the southeastern vortex is weakest). Asymmetric ocean states may account for such differences (Proehl, 1998; Yu et al., 1995). This can explain why only the vortex north of the equator (i.e., the TIV) shows up when the mean flow is superimposed. In addition, the weaker southern part (which lies on the equator) can also explain the secondary frequency peaks of the observed equatorial TIW signals shown in Figures 1a and 1b.

3.3. The Associated Vertical Shear/Mixing

HT15 found that the increases in westward shear drive increased mixing on the leading edge of the TIW warm phase. They demonstrated that horizontal vortex stretching is the dominant process driving the increased shear, supported by a 1-D TIW model settled on the equator with the proposed mechanism. We now investigate the same issues and start directly from the vertically sheared, NE-SW oscillating 17-day TIWs. We again first analyze the TAO data at Eq140W. The shear squared increment associated with, for example, the east-west velocity oscillations at each depth can be defined as

$$S_u'^2 = S_u^2 - S_0^2 = \left(\frac{\partial(\overline{u}+u')}{\partial z}\right)^2 - \left(\frac{\partial \overline{u}}{\partial z}\right)^2 = \left(\frac{\partial u'}{\partial z}\right)^2 + 2\frac{\partial \overline{u}}{\partial z}\frac{\partial u'}{\partial z}. \quad (1)$$

Here for simplification of shear separation, we have defined the 40-day low-passed velocities as the background flow ($\overline{u}$) and assumed the difference between the total and mean velocity as the TIW anomaly ($u' = u - \overline{u}$). Note that since u' is dominated by the 17-day TIWs (Figures 1a and 1b), $S_u'^2$ in (1) could be assumed to represent the shear of the 17-day TIW. In addition, we further signify this shear by a conditional average at specific phases of the 17-day TIW (see caption of Figure 3). The results clearly show that the shear squared is greatly enhanced by the sole westward ATVs (Figure 3a, black solid): It becomes as large as the background value in the upper thermocline (70 m) and is several times larger in the central thermocline (70–125 m). In contrast, the sole eastward ATVs cannot induce in significant shear squared increment (black dashed); instead, the increment is several times smaller than the westward ATVs. For comparison, the increment induced by either the maximum northward or southward ATVs (blue lines) is also several times smaller than the westward ATVs.

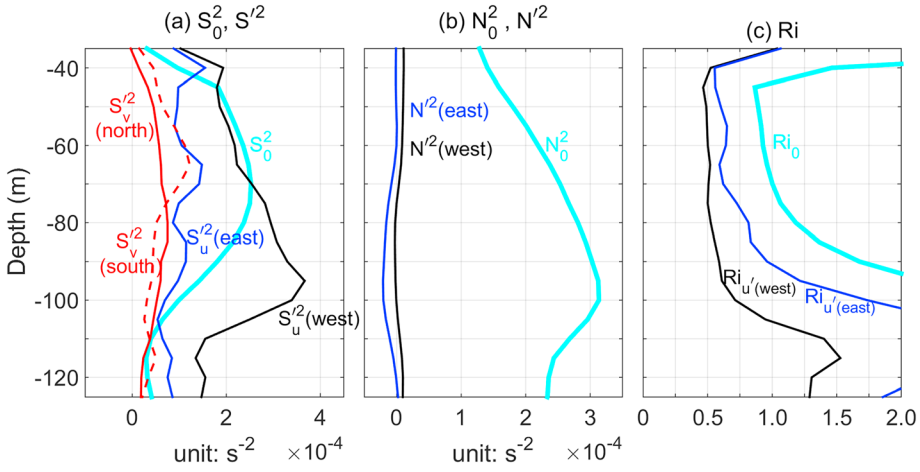

Figure 3. (a) Mean vertical shear squared (S_0^2) of the background flow $\overline{u}$: (cyan), mean shear squared increment by the u component of TIW: $S_u'^2$, averaged at phases of maximum westward (solid black) and eastward (solid blue) anomalous TIW velocities at 45 m; mean shear squared increment by the v component of TIW: $S_v'^2$, averaged at phases of maximum southward (dashed red) and northward (solid red) phases of the 17-day TIW. (b) Mean of the 40-day low-passed buoyancy frequency squared (cyan, N_0^2) and mean of the N'^2 averaged at phases of maximum westward (black solid) and eastward (blue solid) anomalous TIW velocities at 45 m of the 17-day TIW (here N'^2 is the difference between the full N^2 and the 40-day low-passed N^2). (c) Background Ri ($Ri_0 = N_0^2/S_0^2$) and mean Ri corresponding to the solid black and solid blue curves in (a) and (b): $Ri_{u'} = \left(N_0^2 + N'^2\right)/(S_0^2 + S_u'^2)$. Calculated from Tropical Atmosphere-Ocean 1998–2000 data, only those of TIW conditions (120-day low-passed, 30- to 70-m averaged TIWKE > 0.04 m^2/s^2) are used. TIW = tropical instability wave.

The great shear increment by the westward ATVs can be explained simply by wave-mean flow interactions. When the vertical shear of the zonal perturbation has the same direction as that of the background flow (which is westward), that is, for the cases of the surface intensified, westward ATVs of the 17-day TIW (Figure 1f), the shear increment can be enhanced by the positive interaction term $2\frac{\partial \overline{u}}{\partial z}\frac{\partial u'}{\partial z}$. In contrast, the shear increment may be weakened by the negative interaction term when both directions are opposite, as during phases of eastward ATVs. Whereas, the shear increment induced by the meridional oscillations is defined as $S_v'^2 = \left(\frac{\partial v'}{\partial z}\right)^2$, without a wave-mean flow interaction term due to absence of a mean meridional flow.

Subject to variations of the squared buoyancy frequency, N^2, along with the TIW phases, the greatly enhanced shear at phases of maximum westward ATVs may lead to a reduction of the gradient Richardson number $Ri = N^2/S^2$, an indicator for the occurrence of shear instability and thus mixing. Here $N^2 = -\frac{g}{\rho_0}\frac{\partial \rho}{\partial z}$, where g is the gravitational acceleration, ρ_0 = 1,030 kg/m^3 is a reference density, and ρ is the potential density. The N^2 increment averaged at both the westward and eastward phases of the 17-day TIWs are shown in Figure 3b. It can be seen that, on average, the 17-day TIW slightly enhances (decreases) the N^2 at the phases of maximum westward (eastward) ATVs; however, the increment is only about 5% of the total. As a result, Ri is substantially decreased at the phases of maximum westward ATVs due to larger increment of shear and weakly decreased at the phases of maximum eastward ATVs due to smaller increment of shear (Figures 3a and 3c). The decreased Ri at the westward phases, which has a mean magnitude of about 0.5 in the upper thermocline, may be critical for shear instabilities and thus vertical mixing, particularly in sustaining the state of marginal instability in this region (Smyth & Moum, 2013).

This mechanism is then illustrated by the spatial patterns from the reanalysis (Figures 2c and 2d). At 45-m depth, the mean Ri is in the range of marginal instability at the SW phases around the equator, but it is much larger than the critical value ($Ri = 0.25$) at other phases (Figure 2c). This implies that stronger mixing could be expected at the SW phases at the equator. Again, we found that the low Ri in this region is primarily caused by the increment of the total shear (Figure 2d). In contrast, the total shear is reduced at the phases of maximum NE ATVs, because the decrement by the eastward shear exceeds the increment by the northward shear. The change of N^2, which is primarily caused by ATVs' advection of the mean N^2, is relatively small and does not contribute much to the reduction of Ri (not shown).

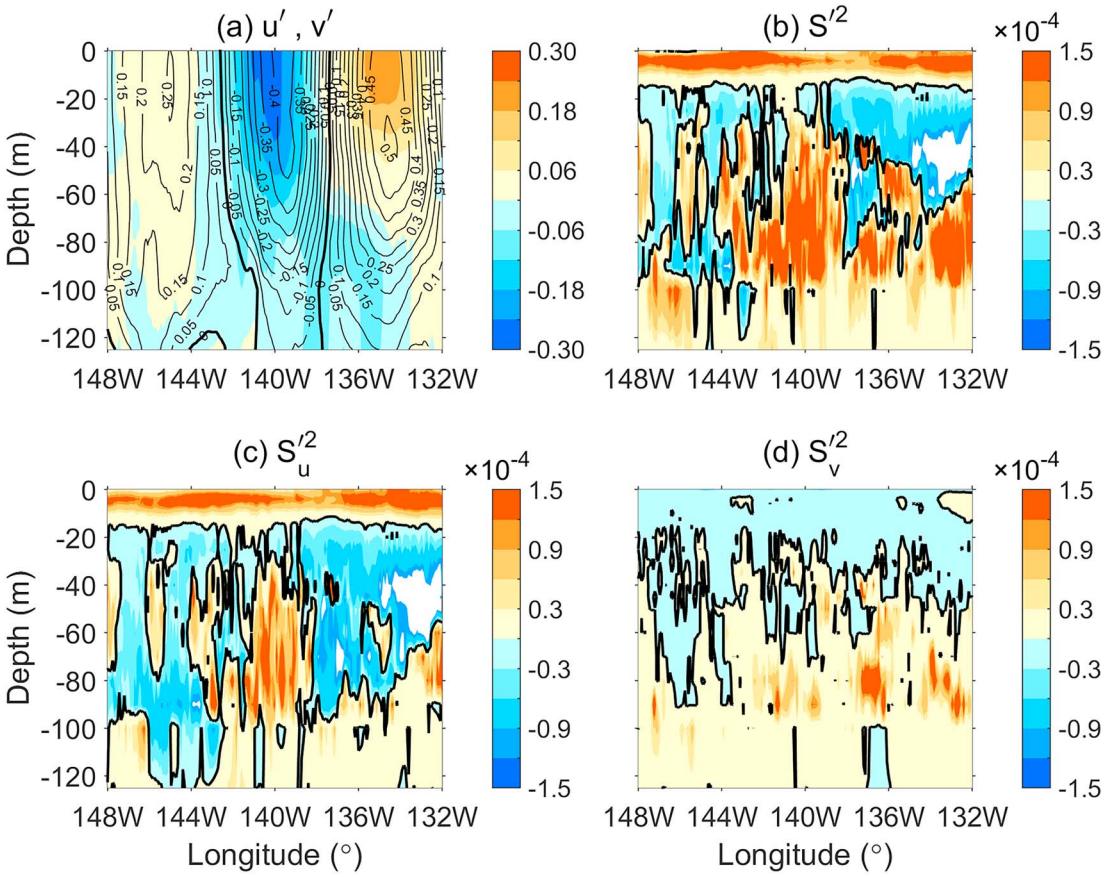

Figure 4. (a) Median of zonal (shading) and meridional (contours) anomalous TIW velocities (m/s), and median of shear squared increment (s^{-2}; isoline of 0 is highlighted); (b) $S_u'^2 + S_v'^2$, (c) $S_u'^2$, and (d) $S_v'^2$ of the 17-day TIW. Calculated at the phases of maximum westward anomalous TIW velocities at 45 m of the Eq140W for October–December 2000. TIW = tropical instability wave.

3.4. The Vertical Structure and Shears

Figure 4a shows the section of averaged ATVs of the 17-day TIW along the equator obtained from the reanalysis. The coherent NE-SW movements between the two components (with phase lag) are clearly illustrated. The shear changes due to the oscillations are shown in Figure 4b. Specifically, the shear squared is greatly enhanced in the upper flank of the thermocline (40–100 m), while slightly weakened above 40 m where both components of ATVs are nearly vertically uniform. In particular, the increment is much larger at the phases of maximum SW ATVs (between 144° and 138°W) than at other phases. It turns out that the *u* component, rather than the *v* component, dominates the shear changes (Figures 4c and 4d). Moreover, it demonstrates that the westward oscillation enhances the shear (Figure 4c; 40–100 m, 142°–138°W) and the eastward oscillation decreases the shear (40–100 m, 147°–143°W and 20–60 m, 137°–133°W).

4. Summary and Discussion

The 17-day TIW, in terms of its associated flows, is identified during La Niña conditions. It is confined within ±4° latitudes and displays NE-SW oscillations, different in structure from the 33-day TIV to the north. It has larger horizontal velocity magnitude than the 33-day TIW at the equator, indicating that the observed TIW-scale oscillations at Eq140W are dominated by this TIW mode. The NE-SW oscillation leads to positive $\overline{u'v'}$, reflecting the nature that the TIWs are (partially) maintained by the barotropic instability of the mean equatorial currents. On the westward phases of this TIW, the surface-intensified, westward-sheared velocity anomalies superimpose on the westward background vertical shear and induce much stronger total shear than other phases; as a result, the *Ri* is greatly reduced and stronger mixing may take place at the equator at these phases. This mechanism may also be applicable to the 33-day TIW because it also shows, though

weak, zonal velocity oscillation at the equator. This mechanism seems to complement HT15's hypothesis, which states that the horizontal vortex stretching leads to enhanced westward shear and hence mixing at the westward phases of TIWs.

The dynamics of the coherent NE-SW oscillation of the 17-day TIW, which also may serve to explain its interannual variability, deserves further exploration. A linearized model of asymmetric equatorial ocean states could indeed produce asymmetric TIWs (Yu et al., 1995), indicating that the NE-SW oscillation might result from the specific asymmetric background that is associated with La Niña and barotopically/baroclinically more unstable conditions. That the total current shear can get greatly enhanced when the eddy shear has the same direction as the mean shear may be an important mechanism for modulation of the vertical mixing/heat transport of the global ocean.

Acknowledgments
This study is supported by the Strategic Priority Research Program and the Key Research Program of Frontier Sciences of CAS (XDA19060102 and QYZDB-SSW-DQC030), the National Natural Science Foundation of China (41606026, 41730534, 41622601, 91858201, and Y72143101B), and the Aoshan Talents Program by the QNML (2017ASTCP-ES03 and 2015ASTP). Data sources (see section 2013) are appreciated. We are grateful to two anonymous reviewers for their very helpful comments and recommendations.

References

Cummings, J. A., and O. M. Smedstad (2013), Variational data assimilation for the Global Ocean. *Data assimilation for atmospheric, oceanic and hydrologic applications* (Vol. 2, chap. 13, pp. 303–343). Berlin, Heidelberg: Springer. https://doi.org/10.1007/978-3-642-35088-7_13

Flament, P. J., Kennan, S. C., Knox, R. A., Niiler, P. P., & Bernstein, R. L. (1996). The three-dimensional structure of an upper ocean vortex in the tropical Pacific Ocean. *Nature*, *383*(6601), 610–613. https://doi.org/10.1038/383610a0

Halpern, D., Knox, R. A., & Luther, D. S. (1988). Observations of 20-day period meridional current oscillations in the upper ocean along the Pacific equator. *Journal of Physical Oceanography*, *18*(11), 1514–1534. https://doi.org/10.1175/1520-0485(1988)018<1514:Oodpmc>2.0.Co;2

Holmes, R. M., & Thomas, L. N. (2015). The modulation of equatorial turbulence by tropical instability waves in a Regional Ocean Model. *Journal of Physical Oceanography*, *45*(4), 1155–1173. https://doi.org/10.1175/JPO-D-14-0209.1

Holmes, R. M., & Thomas, L. N. (2016). Modulation of tropical instability wave intensity by equatorial Kelvin waves. *Journal of Physical Oceanography*, *46*(9), 2623–2643. https://doi.org/10.1175/JPO-D-16-0064.1

Holmes, R. M., Thomas, L. N., Thompson, L., & Darr, D. (2014). Potential vorticity dynamics of tropical instability vortices. *Journal of Physical Oceanography*, *44*(3), 995–1011. https://doi.org/10.1175/JPO-D-13-0157.1

Inoue, R., Lien, R. C., & Moum, J. N. (2012). Modulation of equatorial turbulence by a tropical instability wave. *Journal of Geophysical Research*, *117*, C10009. https://doi.org/10.1029/2011JC007767

Johnson, E. S., & Proehl, J. A. (2004). Tropical instability wave variability in the Pacific and its relation to large-scale currents. *Journal of Physical Oceanography*, *34*(10), 2121–2147. https://doi.org/10.1175/1520-0485(2004)034<2121:Tiwvit>2.0.Co;2

Kennan, S. C., & Flament, P. J. (2000). Observations of a tropical instability vortex. *Journal of Physical Oceanography*, *30*(9), 2277–2301. https://doi.org/10.1175/1520-0485(2000)030<2277:Ooativ>2.0.Co;2

Lien, R. C., D'Asaro, E. A., & Menkes, C. E. (2008). Modulation of equatorial turbulence by tropical instability waves. *Geophysical Research Letters*, *35*, L24607. https://doi.org/10.1029/2008GL035860

Liu, C., Köhl, A., Liu, Z., Wang, F., & Stammer, D. (2016). Deep-reaching thermocline mixing in the equatorial Pacific cold tongue. *Nature Communications*, *7*(1). https://doi.org/10.1038/ncomms11576

Lyman, J. M., Johnson, G. C., & Kessler, W. S. (2007). Distinct 17-and 33-day tropical instability waves in subsurface observations. *Journal of Physical Oceanography*, *37*(4), 855–872. https://doi.org/10.1175/Jpo3023.1

Masina, S., Philander, S. G. H., & Bush, A. B. G. (1999). An analysis of tropical instability waves in a numerical model of the Pacific Ocean: 2. Generation and energetics of the waves. *Journal of Geophysical Research*, *104*(C12), 29,637–29,661. https://doi.org/10.1029/1999JC900226

McCreary, J. P., & Yu, Z. J. (1992). Equatorial dynamics in a 2–1/2-layer model. *Progress in Oceanography*, *29*(1), 61–132. https://doi.org/10.1016/0079-6611(92)90003-I

McPhaden, M. J. (1995). The tropical atmosphere ocean array is completed. *Bulletin of the American Meteorological Society*, *76*(5), 739–744. https://doi.org/10.1175/1520-0477-76.5.739

Menkes, C. E. R., Vialard, J. G., Kennan, S. C., Boulanger, J. P., & Madec, G. V. (2006). A modeling study of the impact of tropical instability waves on the heat budget of the eastern equatorial Pacific. *Journal of Physical Oceanography*, *36*(5), 847–865. https://doi.org/10.1175/Jpo2904.1

Moum, J. N., Lien, R. C., Perlin, A., Nash, J. D., Gregg, M. C., & Wiles, P. J. (2009). Sea surface cooling at the Equator by subsurface mixing in tropical instability waves. *Nature Geoscience*, *2*(11), 761–765. https://doi.org/10.1038/Ngeo657

Moum, J. N., Perlin, A., Nash, J. D., & McPhaden, M. J. (2013). Seasonal sea surface cooling in the equatorial Pacific cold tongue controlled by ocean mixing. *Nature*, *500*(7460), 64–67. https://doi.org/10.1038/Nature12363

Pezzi, L. P., Caltabiano, A., & Challenor, P. (2006). Satellite observations of the Pacific tropical instability wave characteristics and their interannual variability. *International Journal of Remote Sensing*, *27*(8), 1581–1599. https://doi.org/10.1080/01431160500380588

Pezzi, L. P., & Richards, K. J. (2003). Effects of lateral mixing on the mean state and eddy activity of an equatorial ocean. *Journal of Geophysical Research*, *108*(C12), 3371. https://doi.org/10.1029/2003JC001834

Pezzi, L. P., Vialard, J., Richards, K. J., Menkes, C., & Anderson, D. (2004). Influence of ocean-atmosphere coupling on the properties of tropical instability waves. *Geophysical Research Letters*, *31*, L16306. https://doi.org/10.1029/2004GL019995

Proehl, J. A. (1998). The role of meridional flow asymmetry in the dynamics of tropical instability. *Journal of Geophysical Research*, *103*(C11), 24,597–24,618. https://doi.org/10.1029/98JC02372

Qiao, L., & Weisberg, R. H. (1995). Tropical instability wave kinematics—Observations from the Tropical Instability Wave Experiment. *Journal of Geophysical Research*, *100*(C5), 8677–8693. https://doi.org/10.1029/95JC00305

Shinoda, T. (2010). Observed dispersion relation of Yanai waves and 17-day tropical instability waves in the Pacific Ocean. *Science Online Letters on the Atmosphere*, *6*, 17–20. https://doi.org/10.2151/sola.2010-005

Smyth, W. D., & Moum, J. N. (2013). Marginal instability and deep cycle turbulence in the eastern equatorial Pacific Ocean. *Geophysical Research Letters*, *40*, 6181–6185. https://doi.org/10.1002/2013gl058403

Yu, Z. J., McCreary, J. P., & Proehl, J. A. (1995). Meridional asymmetry and energetics of tropical instability waves. *Journal of Physical Oceanography*, *25*(12), 2997–3007. https://doi.org/10.1175/1520-0485(1995)025<2997:Maaeot>2.0.Co;2

Zhang, R. H., & Busalacchi, A. J. (2008). Rectified effects of tropical instability wave (TIW)-induced atmospheric wind feedback in the tropical Pacific. *Geophysical Research Letters*, *35*, L05608. https://doi.org/10.1029/2007GL033028